Am J Physiol Heart Circ Physiol 324: H504–H518, 2023.
First published February 17, 2023; doi:10.1152/ajpheart.00671.2022

american physiological society

AMERICAN JOURNAL OF PHYSIOLOGY
HEART AND CIRCULATORY PHYSIOLOGY

RESEARCH ARTICLE

Integrative Cardiovascular Physiology and Pathophysiology

Multiomics uncover the proinflammatory role of *Trpm4* deletion after myocardial infarction in mice

Mey Boukenna,[1,2,3] Jean-Sébastien Rougier,[1] Parisa Aghagolzadeh,[4] Sylvain Pradervand,[5] Sabrina Guichard,[1] Anne-Flore Hämmerli,[1] Thierry Pedrazzini,[4] and Hugues Abriel[1]

[1]*Institute of Biochemistry and Molecular Medicine and Swiss National Centre of Competence in Research TransCure, University of Bern, Bern, Switzerland;* [2]*Department of Cardiology, Bern University Hospital, Inselspital, University of Bern, Bern, Switzerland;* [3]*Graduate School for Cellular and Biomedical Sciences, University of Bern, Bern, Switzerland;* [4]*Experimental Cardiology Unit, Department of Cardiovascular Medicine, University of Lausanne Medical School, Lausanne, Switzerland; and* [5]*Centre d'Oncologie de Précision, Département d'Oncologie, Centre Hospitalier Universitaire Vaudois, Lausanne, Switzerland*

Abstract

Upon myocardial infarction (MI), ischemia-induced cell death triggers an inflammatory response responsible for removing necrotic material and inducing tissue repair. TRPM4 is a Ca^{2+}-activated ion channel permeable to monovalent cations. Although its role in cardiomyocyte-driven hypertrophy and arrhythmia post-MI has been established, no study has yet investigated its role in the inflammatory process orchestrated by endothelial cells, immune cells, and fibroblasts. This study aims to assess the role of TRPM4 in *1*) survival and cardiac function, *2*) inflammation, and *3*) healing post-MI. We performed ligation of the left coronary artery or sham intervention on 154 *Trpm4* WT or KO mice under isoflurane anesthesia. Survival and echocardiographic functions were monitored up to 5 wk. We collected serum during the acute post-MI phase to analyze proteomes and performed single-cell RNA sequencing on nonmyocytic cells of hearts after 24 and 72 h. Lastly, we assessed chronic fibrosis and angiogenesis. We observed no significant differences in survival or cardiac function, even though our proteomics data showed significantly decreased tissue injury markers (i.e., creatine kinase M and VE-cadherin) in KO serum after 12 h. On the other hand, inflammation, characterized by serum amyloid P component in the serum, higher number of recruited granulocytes, inflammatory monocytes, and macrophages, as well as expression of proinflammatory genes, was significantly higher in KO. This correlated with increased chronic cardiac fibrosis and angiogenesis. Since inflammation and fibrosis are closely linked to adverse remodeling, future therapeutic attempts at inhibiting TRPM4 will need to assess these parameters carefully before proceeding with translational studies.

NEW & NOTEWORTHY Deletion of *Trpm4* increases markers of cardiac and systemic inflammation within the first 24 h after MI, while inducing an earlier fibrotic transition at 72 h and more overall chronic fibrosis and angiogenesis at 5 wk. The descriptive, robust, and methodologically broad approach of this study sheds light on an important caveat that will need to be taken into account in all future therapeutic attempts to inhibit TRPM4 post-MI.

cardiac inflammation; proteomics; transcriptomics; TRPM4

INTRODUCTION

Ischemic heart disease is a leading cause of death affecting ~126 million patients worldwide (1). A majority of these cases is due to chronic atherosclerosis reducing coronary perfusion toward the cardiac muscle. This process can go undiagnosed for decades, until suddenly a triggering event like intense exercise unmasks a mismatch between increased oxygen demand and decreased supply leading to tissue ischemia. When the ischemia lasts longer than a few minutes, cells experience hypoxia and start dying, resulting in myocardial infarction (MI) that is associated with an acute mortality of 34–43% (2). Unfortunately, a considerable proportion of patients that survive MI develop heart failure, which is mainly driven by adverse cardiac remodeling and cardiac fibrosis. Heart failure is associated with again high mortality and low quality of life despite the available pharmacological treatments (3). Thus, the need for novel therapeutic approaches post-MI is dire.

Correspondence: M. Boukenna (may.boukenna@unibe.ch); H. Abriel (hugues.abriel@unibe.ch).
Submitted 28 November 2022 / Revised 10 February 2023 / Accepted 14 February 2023

0363-6135/23 Copyright © 2023 The Authors. Licensed under Creative Commons Attribution CC-BY 4.0.

Published by the American Physiological Society.
Downloaded from journals.physiology.org/journal/ajpheart at Bibliotheque Cantonale Et Universitaire (155.105.125.086) on October 18, 2023.

In recent years, various studies have identified the ion channel TRPM4 as a potential pharmacological target in myocardial infarction (4–6). TRPM4 is a calcium-activated ion channel permeable to monovalent cations such as Na^+, K^+, Li^+, or Cs^+ (7). Its role in cardiac conduction is actively investigated, as many arrhythmic disorders have been linked to *TRPM4* mutations leading to gain or loss of expression and function of the channel (8–11). On increase in intracellular Ca^{2+}, Ca^{2+} binds to TRPM4 inducing a conformational change that opens the channel allowing monovalent cations to move across the plasma membrane. Because of the intra- and extracellular fluid composition, this usually results in a Na^+-influx into the cell, thereby depolarizing the plasma membrane. In addition to the direct effect of Na^+ on the action potential in cardiomyocytes (4, 12–15) and on endothelial cell death via oncosis (15), it also exerts an indirect function by decreasing the driving force for Ca^{2+} ions to enter the cell through Ca^{2+} channels. Since Ca^{2+} is an important second messenger, this indirect effect of TRPM4 on its homeostasis has been shown to have functional implications on cardiomyocyte hypertrophy, macrophage phagocytosis, lymphocyte cytokine production, as well as fibroblast migration and contractility (4, 16–18).

In the heart, most research has concentrated on the role of TRPM4 in cardiomyocytes. For instance, in angiotensin II-induced hypertrophy, cardiomyocyte-specific *Trpm4* KO was shown to increase ventricular hypertrophy (19), whereas in pressure-induced hypertrophy, it decreased left ventricular hypertrophy (20). Similarly, all previous studies investigating the effect of TRPM4 in MI focused on mechanisms related to cardiomyocytes as well. Previous findings suggest that knocking out *Trpm4 1*) protects against ischemia-associated disturbance of Ca^{2+} homeostasis and thus reduces the occurrence of lethal ventricular arrythmias and *2*) increases Ca^{2+}-dependent contractility, improving inotropy on β-adrenergic stimulation (4, 21). Even though most studies suggest a protective effect of knocking out *Trpm4* in MI (4–6), a study by Hedon et al. (22) found an increased mortality in KO mice compared with WT 4 wk post-MI. The diverging observation was attributed to a difference in KO mice.

Thus, findings on how TRPM4 affects survival and heart function diverge and the role of TRPM4 in MI is still poorly understood. Considerable emphasis has been put on cardiomyocytes, even though the heart is made up of only ∼30% of cardiomyocytes and ∼70% of other cells, such as endothelial cells, fibroblasts, immune cells, and smooth muscle cells. Importantly, endothelial cells are the first key players in the inflammatory signaling pathway, inducing infiltration of immune cells into the injured tissue and complement activation. The subsequent inflammatory response mediated mainly by granulocytes, macrophages, and fibroblasts that transdifferentiate into myofibroblasts is crucial for scar tissue formation and thus recovery of cardiac function (23–25). The presence of TRPM4 in these cells prompted us to look beyond cardiomyocytes and investigate the global role of TRPM4 in the inflammatory response post-MI. Here, we therefore present the first detailed characterization of the acute inflammatory processes of *Trpm4* KO compared with WT mice after MI using single-cell RNA sequencing and proteomic approaches. Briefly, we performed LAD ligation, which is a well-established model of ischemic heart disease in mice (26), or sham intervention on *Trpm4* WT and KO mice and sampled blood or cardiac nonmyocytic cells at early time points up to 24 and 72 h, respectively. We observed decreased levels of tissue injury markers such as creatine kinase M (CKM) or vascular endothelial (VE)-cadherin (CDH5) in KO sera compared with those of WT, whereas inflammatory marker serum amyloid P component (APCS), as well as proinflammatory cell types, were upregulated in KO. This increased inflammation in KO correlated with increased fibrosis and angiogenesis at 5 wk after surgery as measured by immunohistochemistry suggesting that deletion of *Trpm4* may have deleterious effects on remodeling post-MI.

MATERIAL AND METHODS

Products

Materials and chemicals used in this study can be found in Table 1.

Mice

The overall experimental setup is visualized in Fig. 1. Male mice (8–12 wk old) were used in all experiments. We used either B6. Cg-Trpm4tm1.2-PG or C57Bl/6N wild-type mice from Janvier Laboratories. We engineered the *Trpm4*$^{-/-}$ (B6. Cg-Trpm4tm1.2-PG) mouse line, which is a constitutive global knockdown of the *Trpm4* gene, by excision of the exon 10, and backcrossing was performed using C57Bl/6N wild-type mice from Janvier Laboratories. All mice were accommodated to the vivarium of the experimental facility for at least 2 wk before any experimental procedure. Mice were kept in cages with a maximum of five mice per cage and with unrestricted access to food and water. All genotypes were controlled again using PCR at the end of the study. Mouse experiments have been approved by the Government Veterinary Office (Lausanne, Switzerland) and conducted according to the University of Lausanne's Institutional Guidelines and the Swiss laws for animal protection, as well as the guidelines from Directive 2010/63/EU of the European Parliament on the protection of animals used for scientific purposes. Accordingly, all euthanasia was performed by neck dislocation after anesthesia by an intraperitoneal injection of a mixture of ketamine-xylazine (65 and 15 mg/kg, respectively), i.e., an injection volume of 0.1 mL/10 g body wt. The minimal number of animals required

Table 1. *List of products, product numbers, and manufacturers*

Product	Cat. No.	Manufacturer
Harris hematoxylin	HHS16	Sigma-Aldrich
AEC staining kit	ab64252	Abcam
Vecta Stain ABC kit	PK7100	Adipogen
Anti-collagen-I antibody	ab21286	Abcam
Anti-CD31 antibody	550274	BD Biosciences
Anti-rabbit biotin	ab7089	Abcam
Anti-rat biotin	559286	BD Biosciences
Cardiomyocyte isolation kit	88281	Thermo Fisher
Calcein-AM	564061	BD Biosciences
DAPI	564907	BD Biosciences
NovaSeq. 6000 S1 Reagent Kit v1.5	20028317	Illumina

Downloaded from journals.physiology.org/journal/ajpheart at Bibliotheque Cantonale Et Universitaire (155.105.125.086) on October 18, 2023.

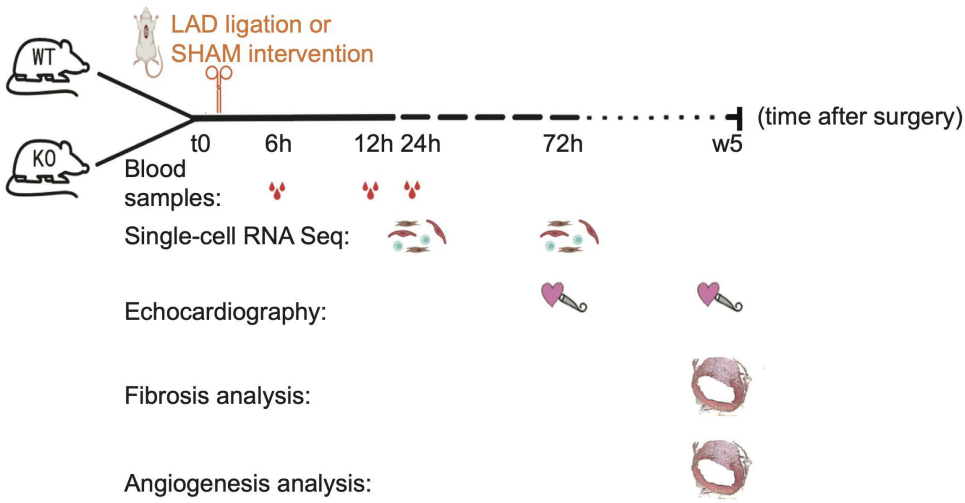

Figure 1. Overview of the study design including blood sampling, in vivo echocardiography, single-cell RNA sequencing, and immunohistochemistry analysis of heart sections to assess fibrosis or angiogenesis using Col1a1 or CD31.

per group was calculated using the online statistical software biostatgv.sentiweb with an effect size of 30%, a binomial distribution using $\sigma = 20$, and type I and type II errors of $\alpha = 0.05$ and $\beta = 0.80$, respectively.

Surgery

All mice included underwent surgery, which was performed by experimenters with multiple years of training in vascular microsurgery. The experimenters performing the surgery (sham or LAD ligation) were blinded for the genotype. The animals were anesthetized by an intraperitoneal injection of a mixture of ketamine-xylazine-acepromazine (65, 15, and 2 mg/kg, respectively), i.e., an injection volume of 0.1 mL/10 g body wt. The skin was incised, the pectoral and intercostal muscles spread, to make an opening in the left third intercostal space. The pericardium was gently opened, and a 7-0 suture was then passed under the left coronary artery ~1–2 mm below the tip of the left atrium. The ligature was then tightened, resulting in a blanching of the portion of the left ventricle supplied by the left coronary artery. The ligature was left in place (permanent ligation) and the animal's rib cage closed (6-0 silk thread). A 5% glucose solution was administered intraperitoneally (0.3–0.5 mL) and a local antiseptic (hydroalcoholic solution) was applied to the skin over the scar. Buprenorphine hydrochloride was administered as an analgesic after surgery as soon as the animal awakened. For sham animals, the same procedure was performed. The only difference was that the suture was not tied around the left coronary artery but only passed under it and removed.

Echocardiography

The mouse was placed under anesthesia with isoflurane 4% in oxygen, 1 L/min for induction, and then maintained under anesthesia via a nose cone using 1–1.5%, 1 L/min. Although under anesthesia, the following parameters were monitored: heart rate, body temperature (with rectal probe), ECG trace, and respiration. The echocardiography images were obtained using a dedicated machine of Visualsonic (Vevo2100) by placing warmed gel on the mouse. The average anesthetic period lasted 10 min. The data analysis was blindly performed, i.e., knowing neither the genotype nor interventional group. Whenever the ejection fraction was above 50% 5 wk post-MI, we controlled immunohistochemistry images (collagen type I staining) to confirm successful infarction via scar identification, as shown in Supplemental Fig. S10 (all Supplemental figures are available at https://doi.org/10.6084/m9.figshare.21937511.v1). Based on the study of Bayat et al. (27), we excluded all mice that had a relative infarct length smaller than 10%. Thus, one mouse in the KO-MI group and one in the WT-MI group had to be excluded because of insufficient MI.

Blood Sampling

We used incision of the tail vein with a sharp blade until we obtained 100 μL of blood. Blood was left to clot at RT for 1 h and then centrifuged at 1,500 *g* for 15 min. The supernatant (serum) was snap frozen.

Nonmyocyte Cells Isolation from Sham-Operated and Infarcted Mouse Hearts

Nonmyocytes were extracted as previously described (28). In short, immediately after neck dislocation, the heart was extracted and rinsed in ice-cold HBSS. Thereafter, ventricles were cut in small (2 × 2 mm) pieces and incubated with thermolysin and papain for 30 min at 37°C under constant gentle shaking and resuspension every 10 min using a Pasteur pipette. After incubation, the reaction was stopped using ice-cold HBSS and large debris were sorted out using a 300-μm mesh. Cardiomyocytes were discarded using low-speed centrifugation (50 *g*) and a 40-μm filter. Cells were subsequently incubated with calcein-AM (live) for 10 min at 37°C, and 4′,6-diamidino-2-phenylindole (DAPI) was used to mark dead cells.

FACS was used to sort live cells. We used a fairly stringent gating FSC area-SSC area, FSC area-FSC height, and SSC area-SSC height to exclude doublets. We used calcein-AM and DAPI to select positive cells and discard dead cells. For each sample, we collected at least 100,000 cells/heart and pooled the sorted cells of four hearts.

Single-Cell RNA Sequencing

A Chromium Next GEM Chip G (10× genomics) was loaded with 12,000 cells, and the libraries were prepared

Downloaded from journals.physiology.org/journal/ajpheart at Bibliotheque Cantonale Et Universitaire (155.105.125.086) on October 18, 2023.

with the Chromium Single Cell 3′ reagents v3.1, strictly following the manufacturer's recommendations. Briefly, an emulsion encapsulating single cells, reverse transcription reagents, and cell barcoding oligonucleotides was generated. After the actual reverse transcription step, the emulsion is broken and double-stranded cDNA generated and amplified in a bulk reaction. This cDNA was fragmented, a P7 sequencing adaptor ligated, and a 3′ gene expression library generated by PCR amplification. Libraries were quantified by a fluorometric method, and their quality was assessed on a fragment analyzer (Agilent Technologies). Cluster generation was performed with an equimolar pool from the resulting libraries using the Illumina Novaseq 6000 Cluster cartridge v1.5. Sequencing was performed on the Illumina Novaseq 6000 using SBS cartridge 100 C v1.5 kit reagents according to 10× Genomics recommendations (28 cycles read1, 10 cycles i7 and i5 index reads and 90 cycles read2).

Processing of 10× Genomics Chromium Single-Cell RNA Seq Data

Fastq files were processed with cell ranger count with default settings (cellranger, 6.0.0) on the mouse genome reference refdata-gex-mm10-2020-A. *filtered_feature_bc_matrix* (cells) data were used for QC analysis with Seurat (3.1.1) in R (R version 3.6.1; 2019-07-05) using default settings. At data loading genes expressed in less than 10 cells were filtered. We kept cells with more than 1,500 UMI counts and more than 600 detected features, as well as less than 30% mitoRNA reads. Data were randomly subset to 3,100 cells/sample. After this step, the standard Seurat pipeline was followed for normalization, integration, scaling, and PCA dimensionality reduction. We use the JackStraw function from Seurat to select the significant principal components ($P < 0.001$, 81 PCs).

Cluster and Subcluster Identification

We used the Seurat *FindNeighbors* method with dims = 1:81, annoy.metric = "cosine" and k.param = 30. *FindClusters* was run at different resolutions. Based on UMAP representation and known gene markers annotation, the resolution 0.8 was chosen. This identified 27 clusters that were labeled according to their cell types. *FindSubCluster* was run on the T cell cluster. Subclustering was also performed on *1*) cells from clusters labeled "fibroblasts" and "epicardial cells" and *2*) cells from clusters labeled "monocytes" and "macrophages." The Seurat pipeline (scaling, PCA, UMAP, FindClusters) was rerun. Based on the JackStraw procedure, 44 PCs were kept for fibroblasts/epicardial cells, and 85 for monocytes/macrophages ($P < 0.001$). For subclustering, we used resolution 0.6.

Differential Gene Expression and Enrichment Analysis

We used Seurat *FindMarkers* (parameter "assay = RNA") with statistical test MAST (29) to identify differentially expressed genes between KO and WT in the different clusters and subclusters. We selected genes with an adjusted P values < 0.05 and an absolute fold change ≥ 2. Gene ontology enrichment analysis was performed with *clusterProfiler* (30).

Differential Proportion Analysis

We used source code from Farbehi et al. (31) for differential proportion analysis (DPA). Null distributions were generated with parameters $n = 10{,}000$ and $P = 1$ for the permutation procedure. P values were adjusted with Benjamini and Hochberg's method.

Proteomics Analysis

Samples (sera) were measured on Evosep LC and timsTOF Pro mass spectrometer. The acquisition mode used was diaPASEF, and samples were analyzed with DIA-NN (available on Github: https://github.com/vdemichev/DiaNN) using default settings with match between runs as previously described (32).

Immunohistochemistry

We performed staining of Col1a1 and CD31 as previously described (24). In short, hearts of mice in *group D* were frozen in OCT. Thereafter, we performed cryosections of 4 μm every 100 μm. The sections were fixed using acetone and air-dried. After quenching for endogenous peroxidase activity with BLOXALL and blocked further with goat serum slides were incubated with primary antibodies (at dilutions 1:100 for anti-CD31 and 1:500 for anti-Col1a1). Slides were subsequently washed with PBS and incubated with biotinylated antibodies, before incubating with VECTASTAIN ABC Reagent. After further washes, heart sections were incubated with AEC Substrate. The reaction was stopped by washing with distilled H_2O. Lastly, sections were counterstained with Harris hematoxylin and slides were mounted. Images were acquired with the Panoramic MIDI II 3DHistech Slide scanner.

RESULTS

Knocking out *Trpm4* Does Not Improve Long-Term Survival 5 wk after MI

We first monitored the survival of *Trpm4* WT and KO mice to assess the influence of the genotype on overall mortality after MI (Fig. 2). Overall 12 out of 57 mice suffered a premature death in the WT-MI group, whereas 7 out of 50 died before euthanasia in the KO-MI group. Although sham-operated WT mice showed no mortality, KO sham mice displayed a mortality of 8.3%. This difference between WT and KO sham was not statistically different. In line with the well-established lethality of MI, we observed a significantly increased mortality of 22.2% in WT mice after MI compared with sham. All WT-MI deaths happened within the first 3 days post-MI and most of them within the first 24 h. Although the survival rate of the KO mice decreased less sharply than that of WT mice in the first 3 days post-MI, it kept decreasing beyond the acute phase, resulting in an overall mortality of 21.2%, which was almost identical to that of WT-MI. We observed no significant difference in survival between both genotypes 5 wk after MI. Thus, we conclude that knocking out *Trpm4* does not improve long-term survival 5 wk after MI.

Knocking out *Trpm4* Does Not Improve Echocardiography Measurements of Cardiac Function after MI

To assess cardiac function, we used cardiac echography and confirmed that MI significantly reduced ejection

Downloaded from journals.physiology.org/journal/ajpheart at Bibliotheque Cantonale Et Universitaire (155.105.125.086) on October 18, 2023.

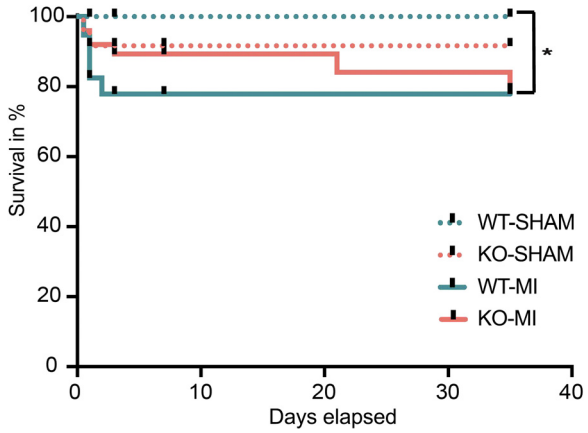

Figure 2. Survival curve for wild-type (WT) and Trpm4 knockout (KO) mice during 5-wk follow-up after LAD ligation. Every short black line represents a censored time point of euthanasia as described in the study design. Kaplan-Meier overall estimation was not significant using Gehan-Breslow-Wilcoxon test with $P = 0.201$. The only significant difference detected was between WT-sham and WT-myocardial infarction (MI) with $P = 0.0221$ using Gehan-Breslow-Wilcoxon test ($n = 23$ for WT-sham, 57 for WT-MI, 24 for KO sham, and 50 for KO-MI). Image was created using a licensed version of BioRender.

fraction and fractional shortening as compared with sham in both genotypes (Fig. 3). Although ejection fraction remained preserved around 45–50% 3 days after MI, it decreased to ~30% in both genotypes 5 wk after MI. We observed a similar phenomenon for the fractional shortening that was ~20–25% 3 days post-MI, whereas it was down to ~15% 5 wk after MI. Despite an initial trend toward an increased LVW-to-BW ratio in *Trpm4* KO mice compared with WT 3 days after MI, this trend was inversed 5 wk after MI. This difference was not accounted for by changes in body weight as visualized in Supplemental Fig. S1. Nevertheless, we observed no significant differences in ejection fraction, LVW-to-BW ratio, fractional shortening, or dyskinetic region/relative infarct size between both genotypes after MI. A table displaying all values measured during echocardiography recordings, including heart rate, which did not differ significantly between genotypes, is provided in the Supplemental Data (see https://doi.org/10.6084/m9.figshare.21937481.v1, https://doi.org/10.6084/m9.figshare.21937499.v1). We conclude that knocking out *Trpm4* does not improve echocardiography measurements of cardiac function after MI.

Serum Proteomics Changes in Acute Phase Post-MI

To assess acute tissue injury and systemic inflammation, we analyzed the sera of the mice at 6, 12, and 24 h after surgery using LC-MS-based proteomics. As represented in Fig. 4*B*, the most highly detected protein in all our samples was albumin, which is the most abundant transport protein in the blood. Six hours after MI, we did not observe any significant differences between WT and KO sera (table provided in Supplemental Data, see https://doi.org/10.6084/m9.figshare.21937487.v1). Twelve hours after MI, KO mice

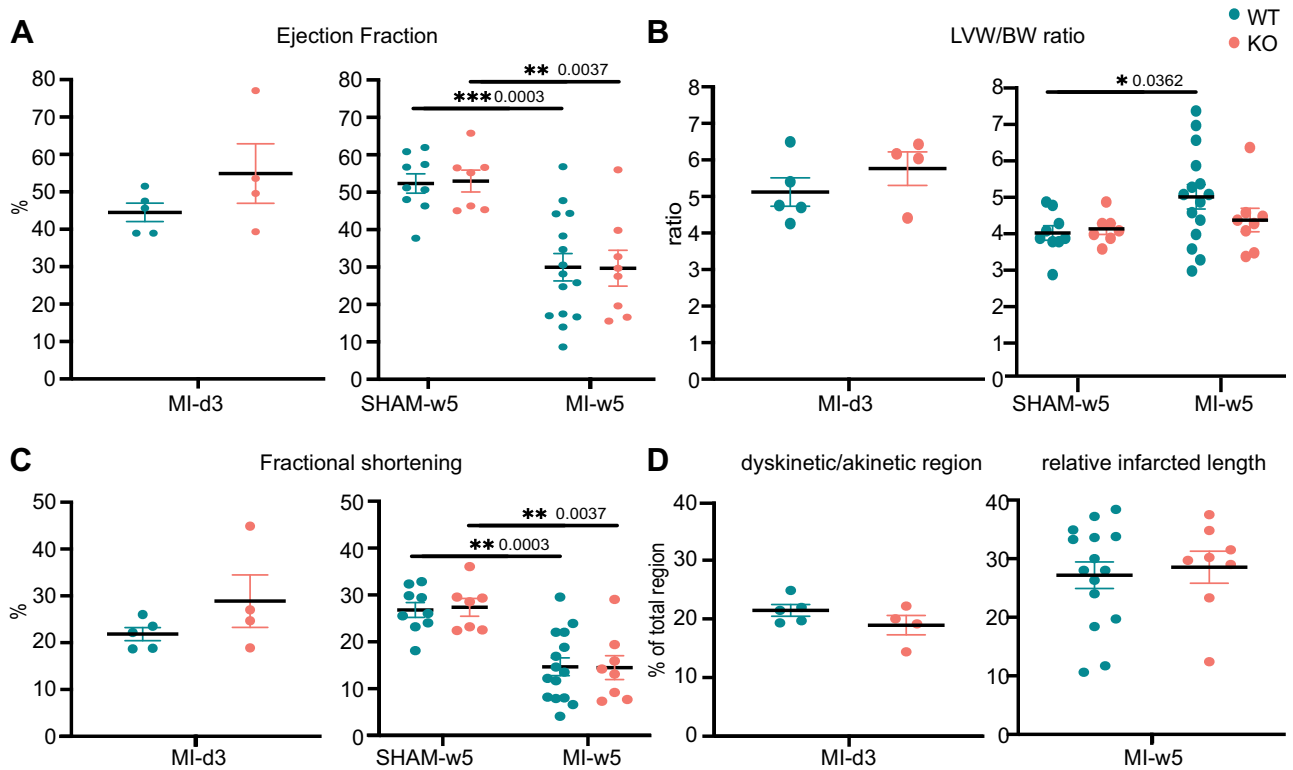

Figure 3. Examination of cardiac performance in wild-type (WT) and Trpm4 knockout (KO) mice 3 days after myocardial infarction (MI) and 5 wk after MI or sham surgery using echocardiography parameters such as ejection fraction (*A*), left ventricular wall-to-body weight (LVW/BW) ratio (*B*), fractional shortening (*C*), and dyskinetic or akinetic region (*D*) at *day 3* or relative infarct length at *week 5*. For this parameter, no sham data are provided since no infarct region or length could be measured. *Statistical significance using Mann-Whitney's test ($n = 5$ for *day 3* WT-MI, and 4 for *day 3* KO-MI; $n = 9$ for *week 5* WT-sham, 15 for *week 5* WT-MI, 7 for *week 5* KO sham, and 8 for *week 5* KO-MI). **$P \leq 0.01$; ***$P \leq 0.001$.

Downloaded from journals.physiology.org/journal/ajpheart at Bibliotheque Cantonale Et Universitaire (155.105.125.086) on October 18, 2023.

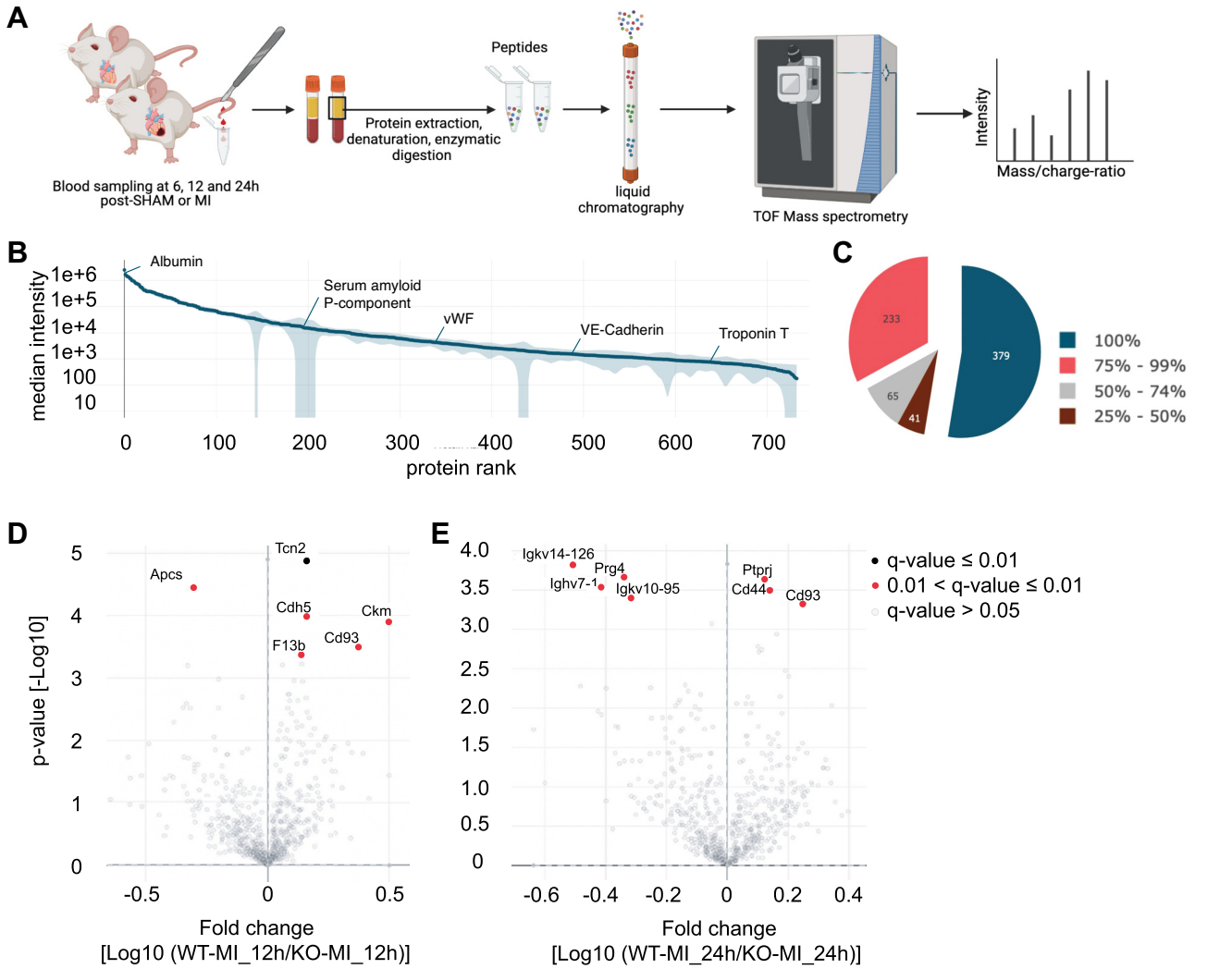

Figure 4. *A*: manual blood sampling and serum isolation followed by automated MS-based proteomics pipeline starting with 1 µL of serum, LC-MS equipment to generate MS raw data and data analysis. *B*: in total, 718 proteins were quantified in this study, covering more than 5 orders of magnitude of MS signal. Examples of frequently applied biomarkers are labeled. *C*: for 144 samples, 718 proteins were detected. The color codes show the protein occurrences in percentage of samples, in which they were detected. *D*: volcano plot comparing the serum proteomes of 11 wild-type (WT) and 11 knockout (KO) mice 12 h after myocardial infarction (MI). *E*: volcano plot comparing the serum proteomes of 6 WT and 13 KO mice 24 h after MI. Legend shows color code highlighting significant fold depending on the q values. Image was created using a licensed version of BioRender.

expressed significantly increased levels of proinflammatory acute phase protein Serum Amyloid P Component (APCS) compared with WT. However, they displayed significantly lower levels of cardiomyocyte injury marker creatine kinase m (CKM), endothelial injury marker VE-cadherin (CDH5), as well as transmembrane receptor CD93, usually found on hematopoietic and endothelial cells, than WT. Moreover, the B-subunit of coagulation factor XIII (F13B) and transcobalamin II (TCN2) were also decreased in KO mice at this time point. Twenty-four hours after MI, CD93 remained lower in KO mice compared with WT, accompanied by surface glycoprotein CD44 and transmembrane receptor Ptprj, all typically expressed on hematopoietic cells. Their soluble form is a marker of injury and inflammation (33–35).

On the other hand, *Trpm4* KO mice sera at 24 h contained more immunoglobulin light chains such as Igkv14-126 and Igkv10-95 and heavy chain Ighv7-1, as well as proreparative proteoglycan 4 (PRG4). Thus, these results are consistent with a stronger inflammatory process and lower tissue injury markers in KO compared with WT mice post-MI.

MI Induces More Proinflammatory and Profibrotic Cells in *Trpm4* KO than WT

Myocardial infarction triggers a complex immune response that involves many cellular and molecular players. To obtain the highest possible resolution into the acute inflammatory cellular response, we performed single-cell RNA sequencing 24 h after sham or MI and 72 h after MI. The cell types found in our nonmyocytic population are shown in Fig. 5, *A*, *C*, and *D*. They comprised endothelial cell (EC) types 1, which are microvascular ECs; type 2, which are arterial ECs; and type 3, which are venous ECs (EC1, EC2, EC3, respectively), interferon-inducible EC (i-EC), fibroblasts (fibro), smooth muscle cells (Sm), pericytes (Pc), granulocytes (Gc), interferon-inducible granulocytes (i-Gc), platelets (Tc),

Downloaded from journals.physiology.org/journal/ajpheart at Bibliotheque Cantonale Et Universitaire (155.105.125.086) on October 18, 2023.

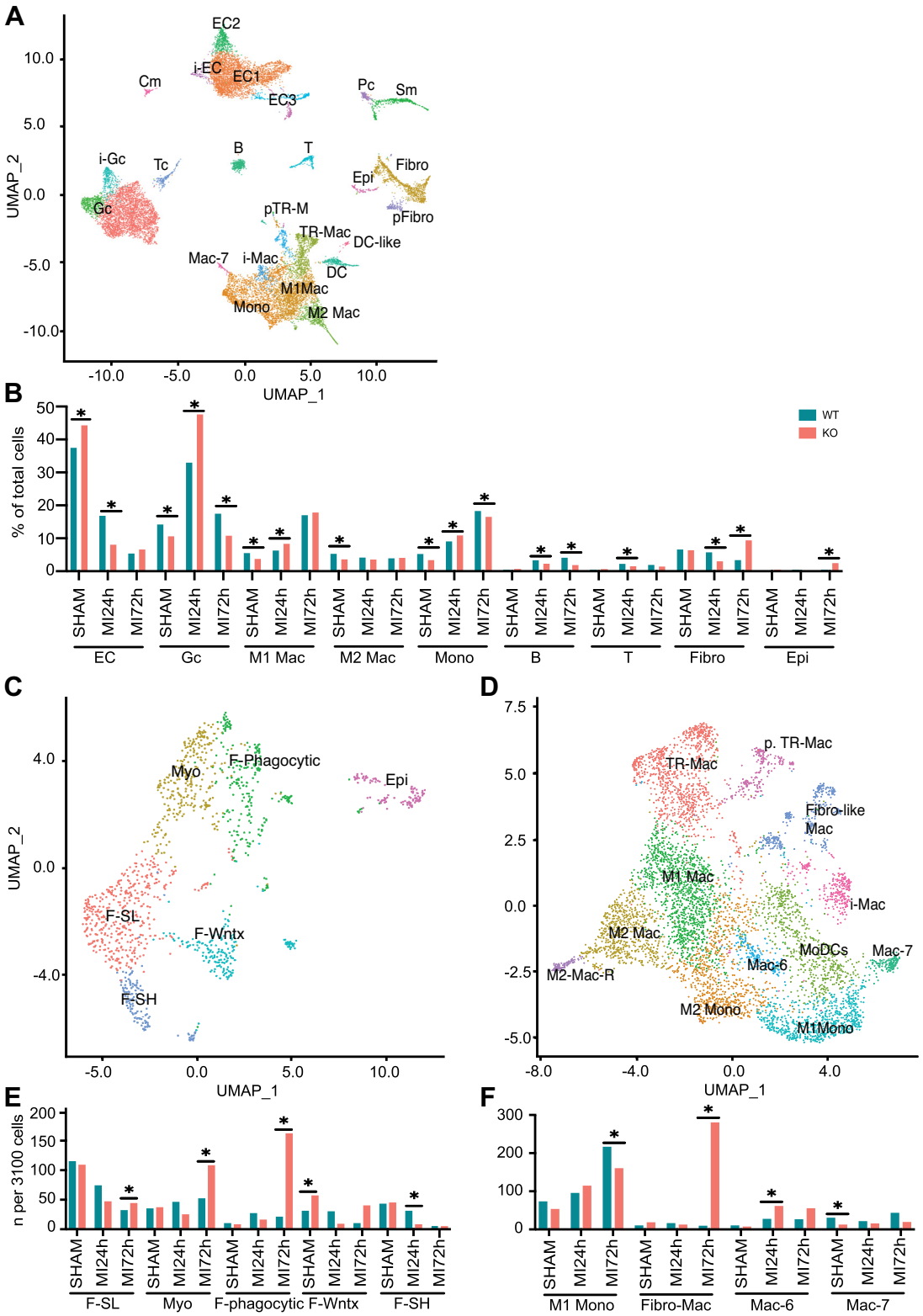

Figure 5. *A*: uniform manifold approximation and projection (UMAP) plot showing detected lineages and subpopulations in noncardiomyocytes (NCM) across conditions. *B*: cell population percentages across conditions with significant (*adjusted $P < 0.05$) differences between genotypes using differential proportion analysis (DPA). *C*: UMAP plot showing subcluster analysis after extracting fibroblasts/epicardial clusters from *A*. *D*: UMAP plot showing subcluster analysis after extracting monocytes/macrophage clusters from *A*. *E*: cell population percentages of cells newly detected in *C*, analogous to *B*. *F*: cell population percentages of cells newly detected in *D*, analogous to *B* ($n = 4$ mice pooled/sample).

Downloaded from journals.physiology.org/journal/ajpheart at Bibliotheque Cantonale Et Universitaire (155.105.125.086) on October 18, 2023.

monocytes (Mono), macrophages (Mac), T and B lymphocytes (abbreviated T and B, respectively), and dendritic cells (DC). Even though we used size filtering and centrifugation to exclude cardiomyocytes (Cm), we could observe a small contamination of the nonmyocytic fraction. A deeper analysis of the monocytes/macrophages showed M1 monocytes (M1 Mono), M2 monocytes (M2 Mono), tissue-resident macrophages (TR-Mac), proliferating TR-Mac (pTR-M), M1 macrophages (M1), M2 macrophages (M2), prorepair genes-high M2 macrophages (M2-Mac-R), interferon-inducible macrophages (i-Mac), Mac-6 macrophages (Mac-6), Mac-7 macrophages (Mac-7), monocyte-derived dendritic cells (MoDCs), and fibroblast-like macrophages (Fibro-like Mac). The subcluster analysis of the fibroblast cluster showed proliferating fibroblasts (pFibro), epicardial cells (Epi), Sca1-high fibroblasts (F-SH), Sca1-low fibroblasts (F-SL), Wnt-expressing fibroblasts (F-Wntx), myofibroblasts (Myo), and catalytic enzymes—high epicardial-derived fibroblasts or myofibroblasts (F-phagocytic). The subcluster analysis of endothelial cells, displayed in Supplemental Fig. S5*C*, additionally revealed inflammatory ECs (infl. EC), angiogenic ECs (Angio), apoptotic ECs (Apo), sprouting EC3s (Sprouting), ECs displaying a transient mesenchymal activation (EndMA), as well as transitioning ECs from EC1 to EC2 (EC1–EC2), EC1 to angiogenic ECs (EC1–Agio) and EC1 to EndMA (EC1–EndMA). Except for M2-Mac-R and Apo, which are not distinct cell types, all these cellular phenotypes have been previously characterized (25, 31, 36–41).

A detailed UMAP visualization of exemplary marker genes per cell population, i.e., *Cdh5* for endothelial cells, *Acta2* for smooth muscle cells, *Kcnj8* for pericytes, *Col1a1* for fibroblasts, *Wt1* for epicardial cells, *Csf3r* for granulocytes, *Mafb* for monocytes and macrophages, *Cd209* for dendritic cells, *Cd3d* for T lymphocytes, and Cd79a for B lymphocytes, can be found in the Supplemental Fig. S3. Twenty-four hours after MI, we measured significantly larger populations of granulocytes, monocytes, and M1 macrophages in KO mice compared with WT. This correlated with an increased number of fibroblasts, myofibroblast and epicardial cells 72 h after MI. Moreover, we detected the appearance of a population of fibroblast-like macrophages (fibro-like Mac), as well as a population of fibroblasts with an immune phenotype (F-phagocytic) 72 h after MI in the KO, which were almost absent in WT mice. This inflammatory phenotype was also visible in KO endothelial cells, where we observed a significantly increased number of inflammatory ECs (infl. EC) at 24 and 72 h after MI, as shown in Supplemental Fig. S5*D*. Overall, these results indicate that MI induces more proinflammatory, and more profibrotic cells in *Trpm4* KO than WT mice.

Trpm4 KO Cells Express Higher Levels of Proinflammatory, Profibrotic, and Proangiogenic Genes

In addition to the valuable and precise information about cell types that can be gained from single-cell RNA sequencing, we used pathway analyses and differential gene expression analyses to get a deeper understanding of the molecular processes at play. At 24 h after MI endothelial cells started expressing higher levels of genes associated to wounding and acute inflammatory response, specifically response to cytokine Il1, leucocyte chemotaxis and adhesion, as well as coagulation. In line with this proinflammatory state, endothelial cells at 24 h, at 72 h, and M1 macrophages and fibroblasts at 72 h showed positive regulation of peptide and protein secretion, as well as catalytic genes such as *Lyz2*. Moreover, genes associated with endopeptidases required for lysosomal processing and proteolysis were also increased. Furthermore, in KO endothelial cells and M1 macrophages genes promoting humoral and B cell immunity were more highly expressed than in WT. This inflammatory response correlated with lower cellular movement, but increased angiogenesis-associated genes. In endothelial cells and fibroblasts, genes for divalent cation homeostasis, more precisely promoting Ca^{2+} mobilization, were increased 72 h after MI compared with WT, but not in M1 nor M2 macrophages. Cell cycle analysis was done separately and can be seen in Supplemental Fig. S4 72 h after MI, it consistently shows more TR-MAC, M1-Mac, M2-Mac, fibroblasts, and epicardial cells in a proliferative state in KO compared with WT. In line with our subcluster analysis, the increased gene expression of cytokine *Il1b* and immune receptor *Fcer1g* in Fig. 6 exemplifies the increasing proinflammatory and immune phenotype of nonimmune cells over time after MI in KO compared with WT.

Taken together, these results indicate that MI induces a higher expression of proinflammatory, profibrotic, and proangiogenic genes in KO than WT mice. They further suggest that Ca^{2+} homeostasis is upregulated in KO compared with WT.

Trpm4 KO Increases Fibrosis and Angiogenesis Post-MI

To assess the long-term consequences of the cell types and pathways affected during acute inflammation, we performed immunostainings on hearts 5 wk after surgery to quantify fibrosis. Figure 7*A* shows the absence of scar tissue after sham surgery in both genotypes. After MI, however, large fibrotic scars are visible. The fibrotic area, including scar tissue and remote fibrosis, extends further in KO compared with WT hearts. The quantification of Col1a1-positive staining as displayed in Fig. 7*B* shows that although MI leads to fibrosis in both genotypes, post-MI fibrosis is significantly higher in KO mice compared with WT. A deeper analysis of infarct, peri-infarct, and remote area as presented in Supplemental Fig. S9 shows that the increase in fibrosis is located throughout the heart tissue. To assess angiogenesis, we used anti-CD31 to stain endothelium. The quantification from Fig. 7*C* shows that KO mice display significantly more endothelial staining than WT mice after MI. Representative images of CD31 staining are also provided in Supplemental Fig. S9. The analysis of angiogenesis per region, performed in Supplemental Fig. S9, shows that angiogenesis is significantly increased in infarct and peri-infarct region.

In line with genes that we found upregulated acutely after MI, these results suggest that *Trpm4* KO promotes fibrosis and angiogenesis post-MI.

DISCUSSION

This study represents the first investigation on the role of TRPM4 in the global inflammatory and healing process following myocardial infarction in mice. The main observations

Downloaded from journals.physiology.org/journal/ajpheart at Bibliotheque Cantonale Et Universitaire (155.105.125.086) on October 18, 2023.

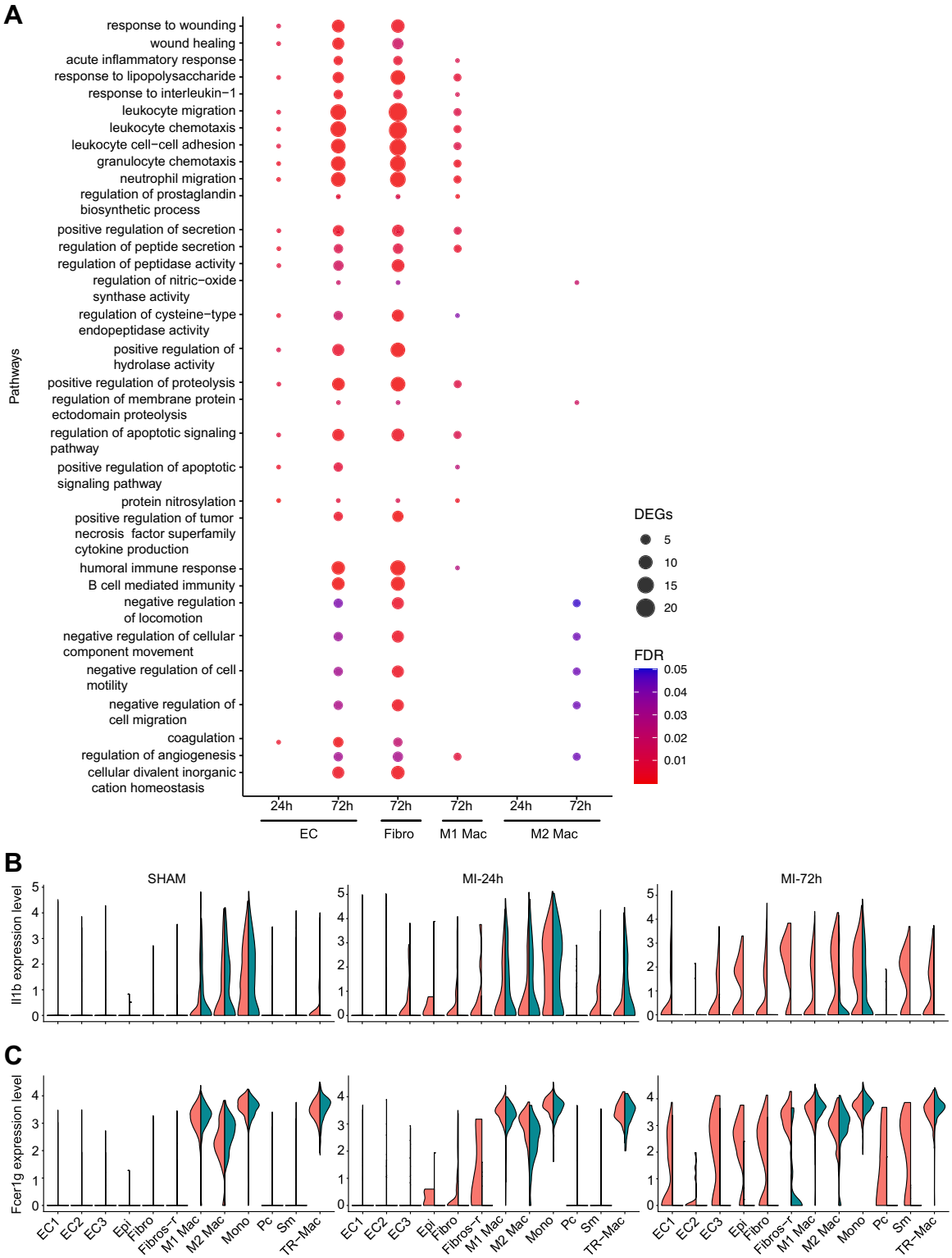

Figure 6. *A*: dot-lot visualizing gene ontology enrichment analysis. The top biological processes significantly enriched in at least 2 knockout (KO) cell populations compared with wild-type (WT) are displayed. The size of the dots represents the number of differentially expressed genes (DEG) and the color code shows the false discovery rate (FDR). *B*: violin plots show the differential gene expression of Il1b in cell populations, in which it was significantly up- or downregulated. *C*: analogous representation for gene Fcer1g (n = 4 mice pooled/sample).

Downloaded from journals.physiology.org/journal/ajpheart at Bibliotheque Cantonale Et Universitaire (155.105.125.086) on October 18, 2023.

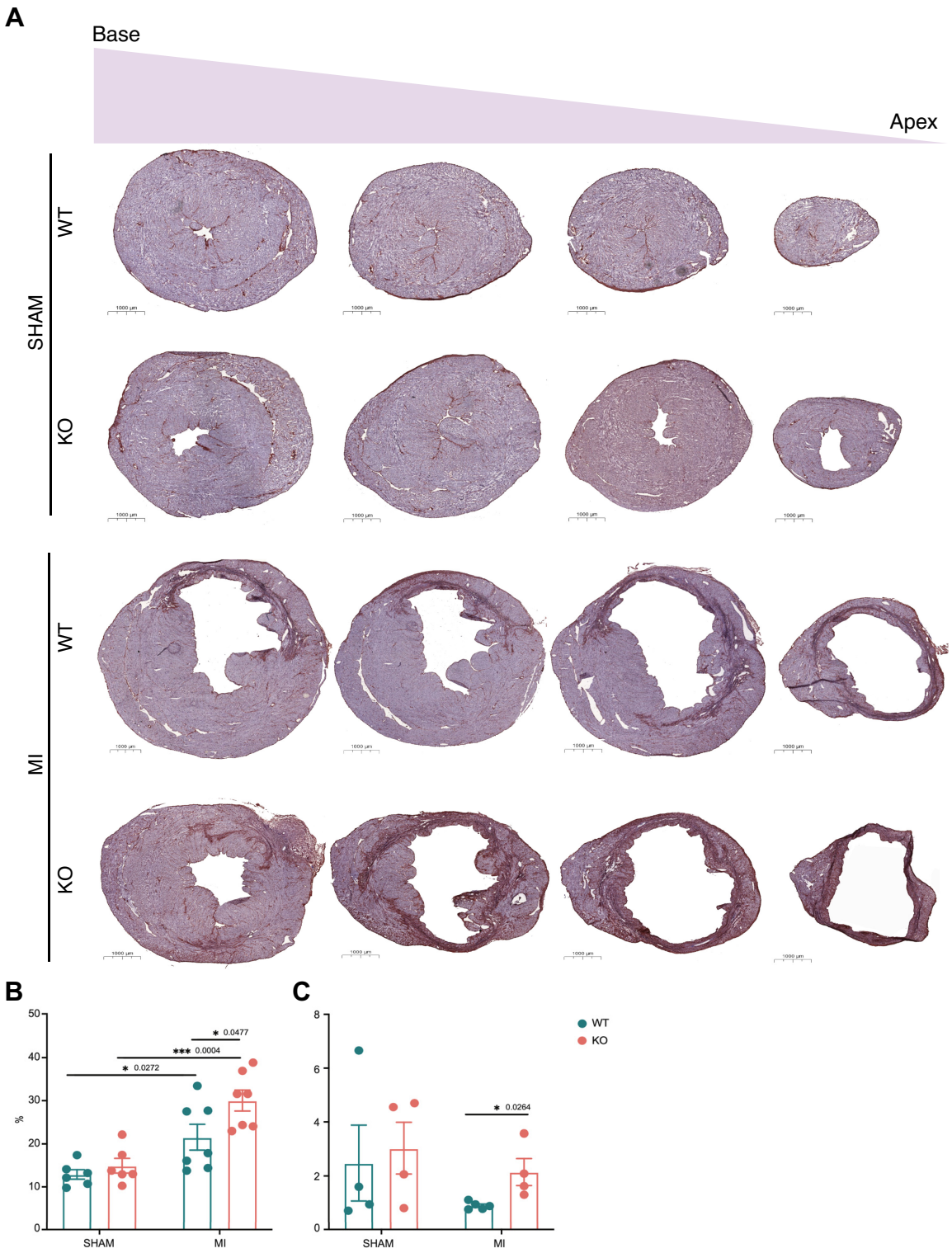

Figure 7. *A*: representative images of transverse heart slices stained with hematoxylin (purple) and immunostaining of Col1a1 (brown). *B*: quantification of fibrosis by calculating Col1a1-positive surface as a percentage of total hematoxylin and eosin (HE)-positive surface (n = 6 for wild-type (WT)-sham, 7 for WT-myocardial infarction (MI), 5 for knockout (KO) sham, and 7 for KO-MI). *C*: analogous quantification of angiogenesis using CD31 as endothelial marker (n = 4 for WT-sham, 5 for WT-MI, 4 for KO sham, and 4 for KO-MI) *Statistical significance using unpaired t test. Unpaired t test was used rather than two-way ANOVA test because of the independence between sham and MI groups. ***$P \leq 0.001$.

Downloaded from journals.physiology.org/journal/ajpheart at Bibliotheque Cantonale Et Universitaire (155.105.125.086) on October 18, 2023.

were that absence of TRPM4 increases acute inflammatory molecular and cellular markers, cardiac fibrosis, and angiogenesis.

Over the course of 5 wk, we did not find significant differences in survival after MI between both genotypes, even though we included more mice than any other study of this type. Jacobs et al. (4), too, did not find any significant differences in long-term post-MI survival between WT and KO mice. However, they did find significantly less mortality in KO mice for the first 7 days post-MI. We found a similar trend in the first week post-MI, which did not reach statistical difference despite including a larger sample size. One key difference between both survival studies is that Jacobs et al. showed a higher mortality in WT mice post-MI (44%) compared with the WT mortality reported in the present study (11%). Such differences in post-MI survival have previously been described and seem inherent to studies employing LAD ligation (42, 43). The lack of difference in survival we observed correlated with our functional data showing no differences in echocardiography parameters at *week 5*, which is also in line with the baseline echocardiography measurements of Jacobs et al. after 10 wk.

The trend showing a decreased early mortality in KO correlated with significantly lower tissue injury markers such as muscle-specific creatine kinase m (CKM) (44, 45) and endothelial-specific VE-cadherin (CDH5) (46–49) in the serum proteomics analysis 12 h after MI. This is in agreement with the findings of Piao et al. (5) showing that *Trpm4* gene deletion and pharmacological inhibition protect cardiomyocytic H9c2 cells from cell death on ischemia-reperfusion injury as mimicked by H_2O_2 incubation. Similarly, Becerra et al. (50) found that silencing or pharmacological blocking of TRPM4 in human umbilical vein endothelial cells significantly reduces lipopolysaccharide-induced cell death.

At the same time, KO was associated with a stronger acute inflammatory phenotype, showing higher levels of the pentameric serum amyloid P component (APCS). APCS is a sensitive marker of inflammation in mice, analogous to CRP in humans (51). It recognizes and opsonizes necrotic, as well as apoptotic cells, and mediates their phagocytosis through type I and type III Fc-receptor γ, also called Fcer1g and Fcer3g, respectively (52). Thus, higher levels of APCS should result in increased opsonization, faster phagocytosis, and quicker resolution of inflammation. Moreover, APCS has been shown to inhibit maladaptive processes such as fibrosis, fibroblast proliferation, and monocyte to fibrocyte transition (52–54). Contrarily to this hypothesis, the *Trpm4* KO mice, which had higher APCS levels, also showed increased fibrosis and more fibroblast proliferation and displayed a fibrocyte-like monocytic population at *day 3* after MI, which was almost absent in WT mice. Since the above-mentioned effects of APCS are mediated by Fcer1g on monocytes and imply a proper monocytic function, we hypothesized that an impaired phagocytic function in KO monocytes and macrophages may explain this unexpected observation. Indeed, a study performed by Serafini et al. (16) demonstrated that deletion of *Trpm4* impairs phagocytic function of macrophages during sepsis in mice. They observed that impaired Ca^{2+} mobilization alters monocytes' and macrophages' phagocytic activity in KO, leading to increased proinflammatory Ly6C^{+} monocytes and proinflammatory cytokine production. Analogous to their results, we found *Trpm4* KO to be associated with upregulated genes responsible for cellular divalent inorganic cation homeostasis, stronger recruitment of proinflammatory neutrophils, M1 monocytes, and macrophages, as well as stronger expression of proinflammatory genes such as *Il1b, Ly6c* (also called *Lyz2*), *S100a8, S100a9, Fcer1g, Cd74, Cd52, C1qb,* and *Tyrobp*. Furthermore, this increased inflammation in *Trpm4* KO mice was associated with marked fibroblast proliferation, and a larger myofibroblast population at *day 3* post-MI. In turn, this profibrotic signature correlated with increased fibrosis as measured by type I collagen staining at 5 wk post-MI. Indeed, it is well established that overshooting inflammation is a driver of cardiac fibrosis after MI (24, 36, 55–57). The increased fibrosis we observe in KO mice does not support the hypothesis of Simard et al. (58) that TRPM4 drives cardiac fibrosis. However, their assumption was based on their in vitro measurement of slower fibroblast growth and decreased transition into myofibroblasts on TRPM4 inhibition. It can be suggested that in the context of MI, this effect is overridden by the role of TRPM4 in inflammation.

The increased fibrosis observed in KO mice from the present study, along with the cardiomyocyte-dependent pathological hypertrophy shown by Hedon et al., are key components of adverse remodeling. Thus, these aspects will need to be evaluated in future therapeutic approaches. As reviewed by Kovács et al., although genetic tools are currently best suited to specifically inhibit TRPM4, there are many TRPM4 inhibitors that could bear great therapeutic potential (59). Compound 4-chloro-2-(1-naphthyloxyacetamido)benzoic acid (NBA) is one of the most potent and effective TRPM4 inhibitors, which suggests it would be the most promising candidate to test in future MI studies (60).

Considering what is known about TRPM4 on calcium homeostasis in endothelial cells and fibroblasts, our findings support the hypothesis that knocking out *Trpm4* promotes calcium influx. Indeed, we found the pathway that upregulates divalent inorganic cation homeostasis increased in KO endothelial cells and fibroblasts compared with WT. Consistent with the findings of Serafini et al. showing that the physiological effect of *Trpm4* KO on calcium influx in murine macrophages is abolished when macrophages are exposed to an inflammatory environment, we did not observe this pathway upregulated in M1 or M2 macrophages.

Along with the above-mentioned proinflammatory genes, our differential gene and pathway analysis also showed increased proangiogenic signatures in KO cardiac cells 3 days after MI. This is consistent with increased angiogenesis measured by CD31 staining 5 wk post-MI, and in line with extensive previous research showing that inflammation is a key promotor of angiogenesis after MI (61). In addition, *Trpm4* silencing or inhibition has also been shown to promote angiogenesis in stroke (62).

Interestingly, there is one protein that has been associated to most of our observations: Factor XIIIa, the last protein of the coagulation cascade that is also crucial for wound healing and adequate cardiac remodeling after MI. It does so by promoting inflammation, increasing neutrophil recruitment, enhancing angiogenesis and Col1a1 synthesis, as well as upregulating fibroblast proliferation. FXIIIa-depleted mice die of cardiac rupture with a 5-day mortality of 100% (63–

Downloaded from journals.physiology.org/journal/ajpheart at Bibliotheque Cantonale Et Universitaire (155.105.125.086) on October 18, 2023.

66). Furthermore, our sera analysis showed elevated factor XIIIb 12 h after MI in WT compared with KO. FXIII is a tetramer consisting of two A- and two B-subunits noncovalently bound. They are also called FXIIIa and FXIIIb, respectively. Once activated by thrombin, Factor XIII releases its two A-subunits to stabilize the fibrin clot. Although the A-subunits are mainly produced in monocytes, macrophages and megakaryocytes/platelets, the B-subunits are synthesized only in hepatocytes. The main function of FXIIIb is to transport the hydrophobic A-subunits within the plasma. Accordingly, all circulating FXIIIa in the plasma is bound to FXIIIb, whereas FXIIIb is present in excess and only half of it is bound to FXIIIa (64). Since FXIII is not an acute phase protein (66), the increased FXIIIb we observe in WT 12 h after MI is unlikely caused by increased synthesis. It seems much more likely to depict a relative increase in its unbound form, which would result from lower FXIIIa levels. Indeed, our single-cell data suggested that proliferating tissue-resident macrophages and fibroblasts expressed less FXIIIa in WT than KO after MI supporting this hypothesis. In line with this, our gene ontology analysis confirmed less genes associated with coagulation cascade in WT compared with KO after MI. Thus, the proteomic analysis, the differential gene analysis, and the pathway analysis would support the hypothesis that MI induces lower levels of FXIIIa in WT compared with KO. Interestingly, FXIIIa is also a transglutaminase. Noll et al. (66) showed that its deposition at endothelial cell junctions decreases endothelial permeability in vitro as well as in vivo after myocardial infarction in rats. Similarly, we also observed increased soluble VE-cadherin in the sera of the WT mice, which is a marker of endothelial barrier disruption and increased permeability on inflammation (67, 68). This suggests that *Trpm4* KO may decrease endothelial permeability after myocardial infarction as has been shown in the brain on stroke (69, 70).

In summary, based on the findings of this study and on the premise that the observations made by Serafini et al. (16) are also valid in sterile inflammation, our leading hypothesis is that, first, *Trpm4* KO leads to increased Ca^{2+}-influx in monocytes on MI-induced inflammatory stimulation, because there is no TRPM4-mediated membrane depolarization that reduces the driving force for Ca^{2+} ions to enter the cell. Second, we postulate that in MI, like in sepsis, sustained inflammation leads to a Ca^{2+} overload during monocytic maturation toward macrophages, which renders the latter unresponsive and reduces their ability to mobilize Ca^{2+}. We hypothesize that this subsequently leads to less efficient efferocytosis and thus an inflammation that is sustained over a longer period of time. Inflammation, in turn, is a key driver for fibrosis and angiogenesis via cellular, autocrine, and paracrine mechanism. Taken together, this would explain the phenotype characterized in our KO mice post-MI. If this line of reasoning is correct, a monocyte-specific *Trpm4* KO would replicate the main findings of our study. Thus, deeper investigation is required to decipher the mechanism behind our observations.

One limitation of this study is that it investigates the role of Trpm4 in mice from a C57Bl/6N strain, whereas Medert et al. demonstrated (21) that the strongest effect of *Trpm4* KO is observed on a 129SvJ background. They proposed that genetic differences, such as the 129SvJ background having two renin genes instead of one, which is associated with higher blood pressure, represent risk factors enhancing the pathological condition of MI. However, it has also been shown that the bacterium S. pneumoniae is highly deadly for 129S2/SvPasCrl substrain mice, whereas C57BL/6 mice are fairly resistant to it (71). Thus, we may expect even more striking cardiac inflammation on MI in 129 mice. This warrants further investigation.

Despite the fact that we included a sample size, which is unprecedently high for any study investigating TRPM4 in MI to this date, the survival analysis we performed did not show any genotype-dependent difference in mortality, contrarily to what has been observed by Jacobs et al (4). In line with their findings, and with the present results showing significantly decreased tissue injury markers in KO, we found a trend toward a lower first-week mortality in *Trpm4* KO. However, to test whether this difference in early survival of ~11% is significant, we would need a sample size of at least 178 mice per group. Inflicting such a high severity grade intervention on such a large number of mice would defy the 3 R (replace, reduce, refine) principles for animal welfare protection, which is why we did not attempt to increase the sample size. The statistical analysis of our echocardiograms at *day 3* would also have benefited from a larger sample size. Furthermore, we decided to include echocardiographic data from all mice with a relative infarct length above 10%. Thus, we detected two mice with small infarct sizes that had ejection fractions above 50%. Our rationale behind the inclusion of small infarct sizes was that a small scar size could suggest a smaller initial MI as well as better post-MI healing. Even if we had excluded them, it would not have significantly altered the statistical results. However, their inclusion increases variability, which poses a limitation by decreasing the power of the study to detect a difference between groups.

Another limitation of this study is that we did not include female mice for the same 3 R reasons. However, the key findings of the present study warrant to be replicated in female mice in the future. Furthermore, since we performed our analysis on serum, we could not measure FXIIIa, as it can only be assessed in plasma (72). Moreover, we used a global KO strategy. Hence, our study offers promising target proteins and cells involved in the proinflammatory phenotype of *Trpm4* KO, but it is impossible to decipher with certainty, via which cells and mechanisms this happens. Although this is a limitation of our experimental design, using a global KO helps to provide an overview of the role of *Trpm4* deletion in post-MI inflammation. We believe this is an important step in identifying potential candidates for cell-specific KO. In addition, a global KO best reflects patients with genetic mutations causing TRPM4 loss of expression. Moreover, based on most currently established therapies, treatment with an inhibitor would also affect all cell types, which is why we aimed to first assess the overall effect. In the future, studies including an inducible knockout or a specific TRPM4 inhibitor, as well as cell type-specific knockouts, will be necessary.

Taken together, our data show that knocking out *Trpm4* does not confer any long-term survival benefit or improved cardiac function over the course of 5 wk. Nevertheless, *Trpm4* KO promotes recruitment of inflammatory cells to the heart and upregulates inflammatory genes in macrophages, endothelial cells, as well as fibroblasts. Moreover, it stimulates proliferation of macrophages and fibroblasts 72 h

Downloaded from journals.physiology.org/journal/ajpheart at Bibliotheque Cantonale Et Universitaire (155.105.125.086) on October 18, 2023.

after MI, which correlates with increased fibrosis and angiogenesis 5 wk post-MI. Thus, we demonstrate that TRPM4 plays a two-sided role in MI. On the one hand, increased fibrosis promotes ventricular stiffness and heart failure, whereas on the other hand increased angiogenesis is associated with improved cardiac recovery post-MI. Therefore, TRPM4 inhibition as has been proposed by many previous studies, bears risks. Targeting TRPM4 in the context of MI should be pondered carefully and approaches that nuance the timing of the inhibition or cellular target may be required. Moreover, these findings prompt the clinically relevant question whether patients with loss-of-expression mutations in the *TRPM4* gene may be at higher risk for adverse remodeling post-MI.

DATA AVAILABILITY

The raw and processed scRNA-seq data can be found under following accession number: GSE210159 (https://www.ncbi.nlm.nih.gov/geo/query/acc.cgi?acc=GSE210159).

SUPPLEMENTAL DATA

The results from the proteomics analyses may be found at https://doi.org/10.6084/m9.figshare.21937484.v1.

Supplemental Figs. S1–S10: https://doi.org/10.6084/m9.figshare.21937511.v1.

Supplemental Tables: https://doi.org/10.6084/m9.figshare.21937481.v1, https://doi.org/10.6084/m9.figshare.21937499.v1, and https://doi.org/10.6084/m9.figshare.21937487.v1.

ACKNOWLEDGMENTS

We thank Anne Catherine Clerc and Drs. Corinne Berthonneche, and Alexandre Sarre from the CAF Facility, University of Lausanne/CHUV; Julien Marquis, Karolina Bojkowska, and Corinne Peter from the GTF Facility University of Lausanne; Omicera GmbH; Dr. Mohamed Nemir from the University of Lausanne for help on immunostainings; Danny Labes from the FACS Facility at the University of Lausanne; Dr. Stefan Müller from the FACS Facility at the University of Bern; and Anastasia Milusev from the DBMR, University of Bern, for readiness to share material.

GRANTS

This work was supported by Swiss National Science Foundation/Swiss Academy of Medical Sciences Grant 323530_199381 (to M.B.), Swiss Heart Foundation grant (to H.A. and M.B.), Novartis Foundation for Biomedical Research Grant 20C196 (to H.A. and M.B.), and NCCR TransCure Grant 51NF40-185544 (to H.A.).

DISCLOSURES

No conflicts of interest, financial or otherwise, are declared by the authors.

AUTHOR CONTRIBUTIONS

M.B. and H.A. conceived and designed research; M.B., P.A., S.G., and A-F.H. performed experiments; M.B. and S.P. analyzed data; M.B., P.A., T.P., and H.A. interpreted results of experiments; M.B. and S.P. prepared figures; M.B. drafted manuscript; M.B., J-S.R., P.A., S.P., T.P., and H.A. edited and revised manuscript; M.B., J-S.R., P.A., S.P., S.G., A-F.H., T.P., and H.A. approved final version of manuscript.

REFERENCES

1. **Khan MA**, **Hashim MJ**, **Mustafa H**, **Baniyas MY**, **Al Suwaidi S**, **AlKatheeri R**, **Alblooshi FMK**, **Almatrooshi M**, **Alzaabi MEH**, **Al Darmaki RS**, **Lootah S.** Global epidemiology of ischemic heart disease: results from the global burden of disease study. *Cureus* 12: e9349, 2020. doi:10.7759/cureus.9349.
2. **Aso S**, **Imamura H**, **Sekiguchi Y**, **Iwashita T**, **Hirano R**, **Ikeda U**, **Okamoto K.** Incidence and mortality of acute myocardial infarction. A population-based study including patients with out-of-hospital cardiac arrest. *Int Heart J* 52: 197–202, 2011. doi:10.1536/ihj.52.197.
3. **Velagaleti RS**, **Pencina MJ**, **Murabito JM**, **Wang TJ**, **Parikh NI**, **D'Agostino RB**, **Levy D**, **Kannel WB**, **Vasan RS.** Long-term trends in the incidence of heart failure after myocardial infarction. *Circulation* 118: 2057–2062, 2008. doi:10.1161/CIRCULATIONAHA.108.784215.
4. **Jacobs G**, **Oosterlinck W**, **Dresselaers T**, **Geenens R**, **Kerselaers S**, **Himmelreich U**, **Herijgers P**, **Vennekens R.** Enhanced β-adrenergic cardiac reserve in Trpm4$^{-/-}$ mice with ischaemic heart failure. *Cardiovasc Res* 105: 330–339, 2015. doi:10.1093/cvr/cvv009.
5. **Piao H**, **Takahashi K**, **Yamaguchi Y**, **Wang C**, **Liu K**, **Naruse K.** Transient receptor potential melastatin-4 is involved in hypoxia-reoxygenation injury in the cardiomyocytes. *PLoS One* 10: e0121703, 2015. doi:10.1371/journal.pone.0121703.
6. **Wang C**, **Chen J**, **Wang M**, **Naruse K**, **Takahashi K.** Role of the TRPM4 channel in mitochondrial function, calcium release, and ROS generation in oxidative stress. *Biochem Biophys Res Commun* 575: 96–98, 2021. doi:10.1016/j.bbrc.2021.08.041.
7. **Guo J**, **She J**, **Zeng W**, **Chen Q**, **Bai XC**, **Jiang Y.** Structures of the calcium-activated, non-selective cation channel TRPM4. *Nature* 552: 205–209, 2017. doi:10.1038/nature24997.
8. **Bianchi B**, **Ozhathil LC**, **Medeiros-Domingo A**, **Gollob MH**, **Abriel H.** Four TRPM4 cation channel mutations found in cardiac conduction diseases lead to altered protein stability. *Front Physiol* 9: 177, 2018. doi:10.3389/fphys.2018.00177.
9. **Syam N**, **Chatel S**, **Ozhathil LC**, **Sottas V**, **Rougier JS**, **Baruteau A**, **Baron E**, **Amarouch MY**, **Daumy X**, **Probst V**, **Schott JJ**, **Abriel H.** Variants of transient receptor potential melastatin member 4 in childhood atrioventricular block. *J Am Heart Assoc* 5: e001625, 2016. doi:10.1161/JAHA.114.001625.
10. **Liu H**, **Chatel S**, **Simard C**, **Syam N**, **Salle L**, **Probst V**, **Morel J**, **Millat G**, **Lopez M**, **Abriel H**, **Schott JJ**, **Guinamard R**, **Bouvagnet P.** Molecular genetics and functional anomalies in a series of 248 Brugada cases with 11 mutations in the TRPM4 channel. *PLoS One* 8: e54131, 2013. doi:10.1371/journal.pone.0054131.
11. **Baruteau AE**, **Probst V**, **Abriel H.** Inherited progressive cardiac conduction disorders. *Curr Opin Cardiol* 30: 33–39, 2015. doi:10.1097/HCO.0000000000000134.
12. **Demion M**, **Thireau J**, **Gueffier M**, **Finan A**, **Khoueiry Z**, **Cassan C**, **Serafini N**, **Aimond F**, **Granier M**, **Pasquié JL**, **Launay P**, **Richard S.** Trpm4 gene invalidation leads to cardiac hypertrophy and electrophysiological alterations. *PLoS One* 9: e115256, 2014. doi:10.1371/journal.pone.0115256.
13. **Guinamard R**, **Bouvagnet P**, **Hof T**, **Liu H**, **Simard C**, **Sallé L.** TRPM4 in cardiac electrical activity. *Cardiovasc Res* 108: 21–30, 2015. doi:10.1093/cvr/cvv213.
14. **Ozhathil LC**, **Rougier JS**, **Arullampalam P**, **Essers MC**, **Ross-Kaschitza D**, **Abriel H.** Deletion of *Trpm4* alters the function of the Na(v)1.5 channel in murine cardiac myocytes. *Int J Mol Sci* 22: 3401, 2021. doi:10.3390/ijms22073401.
15. **Wei S**, **Low SW**, **Poore CP**, **Chen B**, **Gao Y**, **Nilius B**, **Liao P.** Comparison of anti-oncotic effect of TRPM4 blocking antibody in neuron, astrocyte and vascular endothelial cell under hypoxia. *Front Cell Dev Biol* 8: 562584, 2020. doi:10.3389/fcell.2020.562584.
16. **Serafini N**, **Dahdah A**, **Barbet G**, **Demion M**, **Attout T**, **Gautier G**, **Arcos-Fajardo M**, **Souchet H**, **Jouvin MH**, **Vrtovsnik F**, **Kinet JP**, **Benhamou M**, **Monteiro RC**, **Launay P.** The TRPM4 channel controls monocyte and macrophage, but not neutrophil, function for survival in sepsis. *J Immunol* 189: 3689–3699, 2012. doi:10.4049/jimmunol.1102969.

Downloaded from journals.physiology.org/journal/ajpheart at Bibliotheque Cantonale Et Universitaire (155.105.125.086) on October 18, 2023.

17. **Launay P**, **Fleig A**, **Perraud AL**, **Scharenberg AM**, **Penner R**, **Kinet JP.** TRPM4 is a Ca^{2+}-activated nonselective cation channel mediating cell membrane depolarization. *Cell* 109: 397–407, 2002. doi:10.1016/s0092-8674(02)00719-5.
18. **Cáceres M**, **Ortiz L**, **Recabarren T**, **Romero A**, **Colombo A**, **Leiva-Salcedo E**, **Varela D**, **Rivas J**, **Silva I**, **Morales D**, **Campusano C**, **Almarza O**, **Simon F**, **Toledo H**, **Park KS**, **Trimmer JS**, **Cerda O.** TRPM4 is a novel component of the adhesome required for focal adhesion disassembly, migration and contractility. *PLoS One* 10: e0130540, 2015. doi:10.1371/journal.pone.0130540.
19. **Kecskés M**, **Jacobs G**, **Kerselaers S**, **Syam N**, **Menigoz A**, **Vangheluwe P**, **Freichel M**, **Flockerzi V**, **Voets T**, **Vennekens R.** The Ca^{2+}-activated cation channel TRPM4 is a negative regulator of angiotensin II-induced cardiac hypertrophy. *Basic Res Cardiol* 110: 43, 2015. doi:10.1007/s00395-015-0501-x.
20. **Guo Y**, **Yu ZY**, **Wu J**, **Gong H**, **Kesteven S**, **Iismaa SE**, **Chan AY**, **Holman S**, **Pinto S**, **Pironet A**, **Cox CD**, **Graham RM**, **Vennekens R**, **Feneley MP**, **Martinac B.** The Ca^{2+}-activated cation channel TRPM4 is a positive regulator of pressure overload-induced cardiac hypertrophy. *eLife* 10: e66582, 2021. doi:10.7554/eLife.66582.
21. **Medert R**, **Pironet A**, **Bacmeister L**, **Segin S**, **Londoño JEC**, **Vennekens R**, **Freichel M.** Genetic background influences expression and function of the cation channel TRPM4 in the mouse heart. *Basic Res Cardiol* 115: 70, 2020. doi:10.1007/s00395-020-00831-x.
22. **Hedon C**, **Lambert K**, **Chakouri N**, **Thireau J**, **Aimond F**, **Cassan C**, **Bideaux P**, **Richard S**, **Faucherre A**, **Le Guennec JY**, **Demion M.** New role of TRPM4 channel in the cardiac excitation-contraction coupling in response to physiological and pathological hypertrophy in mouse. *Prog Biophys Mol Biol* 159: 105–117, 2021. doi:10.1016/j.pbiomolbio.2020.09.006.
23. **Frantz S**, **Nahrendorf M.** Cardiac macrophages and their role in ischaemic heart disease. *Cardiovasc Res* 102: 240–248, 2014. doi:10.1093/cvr/cvu025.
24. **Sager HB**, **Hulsmans M**, **Lavine KJ**, **Moreira MB**, **Heidt T**, **Courties G**, **Sun Y**, **Iwamoto Y**, **Tricot B**, **Khan OF**, **Dahlman JE**, **Borodovsky A**, **Fitzgerald K**, **Anderson DG**, **Weissleder R**, **Libby P**, **Swirski FK**, **Nahrendorf M.** Proliferation and recruitment contribute to myocardial macrophage expansion in chronic heart failure. *Circ Res* 119: 853–864, 2016. doi:10.1161/CIRCRESAHA.116.309001.
25. **Forte E**, **Skelly DA**, **Chen M**, **Daigle S**, **Morelli KA**, **Hon O**, **Philip VM**, **Costa MW**, **Rosenthal NA**, **Furtado MB.** Dynamic interstitial cell response during myocardial infarction predicts resilience to rupture in genetically diverse mice. *Cell Rep* 30: 3149–3163.e6, 2020. doi:10.1016/j.celrep.2020.02.008.
26. **Oh JG**, **Kho C**, **Hajjar RJ**, **Ishikawa K.** Experimental models of cardiac physiology and pathology. *Heart Fail Rev* 24: 601–615, 2019. doi:10.1007/s10741-019-09769-2.
27. **Bayat H**, **Swaney JS**, **Ander AN**, **Dalton N**, **Kennedy BP**, **Hammond HK**, **Roth DM.** Progressive heart failure after myocardial infarction in mice. *Basic Res Cardiol* 97: 206–213, 2002. doi:10.1007/s003950200013.
28. **Pinto AR**, **Chandran A**, **Rosenthal NA**, **Godwin JW.** Isolation and analysis of single cells from the mouse heart. *J Immunol Methods* 393: 74–80, 2013. doi:10.1016/j.jim.2013.03.012.
29. **Finak G**, **McDavid A**, **Yajima M**, **Deng J**, **Gersuk V**, **Shalek AK**, **Slichter CK**, **Miller HW**, **McElrath MJ**, **Prlic M**, **Linsley PS**, **Gottardo R.** MAST: a flexible statistical framework for assessing transcriptional changes and characterizing heterogeneity in single-cell RNA sequencing data. *Genome Biol* 16: 278, 2015. doi:10.1186/s13059-015-0844-5.
30. **Yu G**, **Wang LG**, **Han Y**, **He QY.** clusterProfiler: an R package for comparing biological themes among gene clusters. *OMICS* 16: 284–287, 2012. doi:10.1089/omi.2011.0118.
31. **Farbehi N**, **Patrick R**, **Dorison A**, **Xaymardan M**, **Janbandhu V**, **Wystub-Lis K**, **Ho JW**, **Nordon RE**, **Harvey RP.** Single-cell expression profiling reveals dynamic flux of cardiac stromal, vascular and immune cells in health and injury. *eLife* 8, 2019. doi:10.7554/eLife.43882.
32. **Demichev V**, **Messner CB**, **Vernardis SI**, **Lilley KS**, **Ralser M.** DIA-NN: neural networks and interference correction enable deep proteome coverage in high throughput. *Nat Methods* 17: 41–44, 2020. doi:10.1038/s41592-019-0638-x.
33. **Youn JC**, **Yu HT**, **Jeon JW**, **Lee HS**, **Jang Y**, **Park YW**, **Park YB**, **Shin EC**, **Ha JW.** Soluble CD93 levels in patients with acute myocardial infarction and its implication on clinical outcome. *PLoS One* 9: e96538, 2014. doi:10.1371/journal.pone.0096538.
34. **Muqaku B**, **Eisinger M**, **Meier SM**, **Tahir A**, **Pukrop T**, **Haferkamp S**, **Slany A**, **Reichle A**, **Gerner C.** Multi-omics analysis of serum samples demonstrates reprogramming of organ functions via systemic calcium mobilization and platelet activation in metastatic melanoma. *Mol Cell Proteomics* 16: 86–99, 2017. doi:10.1074/mcp.M116.063313.
35. **Mashayekhi F**, **Aryaee H**, **Mirzajani E**, **Yasin AA**, **Fathi A.** Soluble CD44 concentration in the serum and peritoneal fluid samples of patients with different stages of endometriosis. *Arch Gynecol Obstet* 292: 641–645, 2015. doi:10.1007/s00404-015-3654-9.
36. **Haider N**, **Boscá L**, **Zandbergen HR**, **Kovacic JC**, **Narula N**, **González-Ramos S**, **Fernandez-Velasco M**, **Agrawal S**, **Paz-García M**, **Gupta S**, **DeLeon-Pennell K**, **Fuster V**, **Ibañez B**, **Narula J.** Transition of macrophages to fibroblast-like cells in healing myocardial infarction. *J Am Coll Cardiol* 74: 3124–3135, 2019. doi:10.1016/j.jacc.2019.10.036.
37. **Dick SA**, **Macklin JA**, **Nejat S**, **Momen A**, **Clemente-Casares X**, **Althagafi MG**, **Chen J**, **Kantores C**, **Hosseinzadeh S**, **Aronoff L**, **Wong A**, **Zaman R**, **Barbu I**, **Besla R**, **Lavine KJ**, **Razani B**, **Ginhoux F**, **Husain M**, **Cybulsky MI**, **Robbins CS**, **Epelman S.** Publisher correction: self-renewing resident cardiac macrophages limit adverse remodeling following myocardial infarction. *Nat Immunol* 20: 664, 2019. doi:10.1038/s41590-019-0363-8.
38. **Cochain C**, **Vafadarnejad E**, **Arampatzi P**, **Pelisek J**, **Winkels H**, **Ley K**, **Wolf D**, **Saliba AE**, **Zernecke A.** Single-cell RNA-Seq reveals the transcriptional landscape and heterogeneity of aortic macrophages in murine atherosclerosis. *Circ Res* 122: 1661–1674, 2018. doi:10.1161/CIRCRESAHA.117.312509.
39. **McCracken IR**, **Dobie R**, **Bennett M**, **Passi R**, **Beqqali A**, **Henderson NC**, **Mountford JC**, **Riley PR**, **Ponting CP**, **Smart N**, **Brittan M**, **Baker AH.** Mapping the developing human cardiac endothelium at single-cell resolution identifies MECOM as a regulator of arteriovenous gene expression. *Cardiovasc Res* 118: 2960–2972, 2022. doi:10.1093/cvr/cvac023.
40. **Tombor LS**, **John D**, **Glaser SF**, **Luxán G**, **Forte E**, **Furtado M**, **Rosenthal N**, **Baumgarten N**, **Schulz MH**, **Wittig J**, **Rogg EM**, **Manavski Y**, **Fischer A**, **Muhly-Reinholz M**, **Klee K**, **Looso M**, **Selignow C**, **Acker T**, **Bibli SI**, **Fleming I**, **Patrick R**, **Harvey RP**, **Abplanalp WT**, **Dimmeler S.** Single cell sequencing reveals endothelial plasticity with transient mesenchymal activation after myocardial infarction. *Nat Commun* 12: 681, 2021. doi:10.1038/s41467-021-20905-1.
41. **Kalucka J**, **de Rooij L**, **Goveia J**, **Rohlenova K**, **Dumas SJ**, **Meta E et al**. Single-cell transcriptome atlas of murine endothelial cells. *Cell* 180: 764–779.e20, 2020. doi:10.1016/j.cell.2020.01.015.
42. **Ahn D**, **Cheng L**, **Moon C**, **Spurgeon H**, **Lakatta EG**, **Talan MI.** Induction of myocardial infarcts of a predictable size and location by branch pattern probability-assisted coronary ligation in C57BL/6 mice. *Am J Physiol Heart Circ Physiol* 286: H1201–H1207, 2004. doi:10.1152/ajpheart.00862.2003.
43. **Gao E**, **Koch WJ.** A novel and efficient model of coronary artery ligation in the mouse. *Methods Mol Biol* 1037: 299–311, 2013. doi:10.1007/978-1-62703-505-7_17.
44. **Bhayana V**, **Henderson AR.** Biochemical markers of myocardial damage. *Clin Biochem* 28: 1–29, 1995. doi:10.1016/0009-9120(94)00065-4.
45. **Pan Y**, **Wang L**, **Xie Y**, **Tan Y**, **Chang C**, **Qiu X**, **Li X.** Characterization of differentially expressed plasma proteins in patients with acute myocardial infarction. *J Proteomics* 227: 103923, 2020. doi:10.1016/j.jprot.2020.103923.
46. **Yu WK**, **McNeil JB**, **Wickersham NE**, **Shaver CM**, **Bastarache JA**, **Ware LB.** Vascular endothelial cadherin shedding is more severe in sepsis patients with severe acute kidney injury. *Crit Care* 23: 18, 2019. doi:10.1186/s13054-019-2315-y.
47. **Soeki T**, **Tamura Y**, **Shinohara H**, **Sakabe K**, **Onose Y**, **Fukuda N.** Elevated concentration of soluble vascular endothelial cadherin is associated with coronary atherosclerosis. *Circ J* 68: 1–5, 2004. doi:10.1253/circj.68.1.
48. **Zhang RY**, **Liu YY**, **Li L**, **Cui W**, **Zhao KJ**, **Huang WC**, **Gu XW**, **Liu W**, **Wu J**, **Min D**, **Mao EQ**, **Tang YQ.** Increased levels of soluble vascular endothelial cadherin are associated with poor outcome in severe sepsis. *J Int Med Res* 38: 1497–1506, 2010. doi:10.1177/147323001003800433.

Downloaded from journals.physiology.org/journal/ajpheart at Bibliotheque Cantonale Et Universitaire (155.105.125.086) on October 18, 2023.

49. **Herren B**, **Levkau B**, **Raines EW**, **Ross R.** Cleavage of beta-catenin and plakoglobin and shedding of VE-cadherin during endothelial apoptosis: evidence for a role for caspases and metalloproteinases. *Mol Biol Cell* 9: 1589–1601, 1998. doi:10.1091/mbc.9.6.1589.
50. **Becerra A**, **Echeverría C**, **Varela D**, **Sarmiento D**, **Armisén R**, **Nuñez-Villena F**, **Montecinos M**, **Simon F.** Transient receptor potential melastatin 4 inhibition prevents lipopolysaccharide-induced endothelial cell death. *Cardiovasc Res* 91: 677–684, 2011. doi:10.1093/cvr/cvr135.
51. **Ku NO**, **Mortensen RF.** The mouse C-reactive protein (CRP) gene is expressed in response to IL-1 but not IL-6. *Cytokine* 5: 319–326, 1993. doi:10.1016/1043-4666(93)90063-b.
52. **Mold C**, **Gresham HD**, **Du Clos TW.** Serum amyloid P component and C-reactive protein mediate phagocytosis through murine Fc gamma Rs. *J Immunol* 166: 1200–1205, 2001. doi:10.4049/jimmunol.166.2.1200.
53. **Bottazzi B**, **Inforzato A**, **Messa M**, **Barbagallo M**, **Magrini E**, **Garlanda C**, **Mantovani A.** The pentraxins PTX3 and SAP in innate immunity, regulation of inflammation and tissue remodelling. *J Hepatol* 64: 1416–1427, 2016. doi:10.1016/j.jhep.2016.02.029.
54. **Pilling D**, **Buckley CD**, **Salmon M**, **Gomer RH.** Inhibition of fibrocyte differentiation by serum amyloid P. *J Immunol* 171: 5537–5546, 2003. doi:10.4049/jimmunol.171.10.5537.
55. **Liu J**, **Wang H**, **Li J.** Inflammation and inflammatory cells in myocardial infarction and reperfusion injury: a double-edged sword. *Clin Med Insights Cardiol* 10: 79–84, 2016. doi:10.4137/CMC.S33164.
56. **Prabhu SD**, **Frangogiannis NG.** The biological basis for cardiac repair after myocardial infarction: from inflammation to fibrosis. *Circ Res* 119: 91–112, 2016. doi:10.1161/CIRCRESAHA.116.303577.
57. **Dutta P**, **Nahrendorf M.** Monocytes in myocardial infarction. *Arterioscler Thromb Vasc Biol* 35: 1066–1070, 2015. doi:10.1161/ATVBAHA.114.304652.
58. **Simard C**, **Magaud C**, **Adjlane R**, **Dupas Q**, **Sallé L**, **Manrique A**, **Bois P**, **Faivre JF**, **Guinamard R.** TRPM4 non-selective cation channel in human atrial fibroblast growth. *Pflugers Arch* 472: 1719–1732, 2020. doi:10.1007/s00424-020-02476-0.
59. **Kovács ZM**, **Dienes C**, **Hézső T**, **Almássy J**, **Magyar J**, **Bányász T**, **Nánási PP**, **Horváth B**, **Szentandrássy N.** Pharmacological modulation and (patho)physiological roles of TRPM4 channel-part 1: modulation of TRPM4. *Pharmaceuticals (Basel)* 15: 81, 2022. doi:10.3390/ph15010081.
60. **Arullampalam P**, **Preti B**, **Ross-Kaschitza D**, **Lochner M**, **Rougier JS**, **Abriel H.** Species-specific effects of cation channel TRPM4 small-molecule inhibitors. *Front Pharmacol* 12: 712354, 2021. doi:10.3389/fphar.2021.712354.
61. **Nian M**, **Lee P**, **Khaper N**, **Liu P.** Inflammatory cytokines and postmyocardial infarction remodeling. *Circ Res* 94: 1543–1553, 2004. doi:10.1161/01.RES.0000130526.20854.fa.
62. **Loh KP**, **Ng G**, **Yu CY**, **Fhu CK**, **Yu D**, **Vennekens R**, **Nilius B**, **Soong TW**, **Liao P.** TRPM4 inhibition promotes angiogenesis after ischemic stroke. *Pflugers Arch* 466: 563–576, 2014. doi:10.1007/s00424-013-1347-4.
63. **Nahrendorf M**, **Hu K**, **Frantz S**, **Jaffer FA**, **Tung CH**, **Hiller KH**, **Voll S**, **Nordbeck P**, **Sosnovik D**, **Gattenlöhner S**, **Novikov M**, **Dickneite G**, **Reed GL**, **Jakob P**, **Rosenzweig A**, **Bauer WR**, **Weissleder R**, **Ertl G.** Factor XIII deficiency causes cardiac rupture, impairs wound healing, and aggravates cardiac remodeling in mice with myocardial infarction. *Circulation* 113: 1196–1202, 2006. doi:10.1161/CIRCULATIONAHA.105.602094.
64. **Muszbek L**, **Bereczky Z**, **Bagoly Z**, **Komáromi I**, **Katona E.** Factor XIII: a coagulation factor with multiple plasmatic and cellular functions. *Physiol Rev* 91: 931–972, 2011. doi:10.1152/physrev.00016.2010.
65. **Dickneite G**, **Herwald H**, **Korte W**, **Allanore Y**, **Denton CP**, **Matucci Cerinic M.** Coagulation factor XIII: a multifunctional transglutaminase with clinical potential in a range of conditions. *Thromb Haemost* 113: 686–697, 2015. doi:10.1160/TH14-07-0625.
66. **Penzes K**, **Hurjak B**, **Katona E**, **Becs G**, **Balla J**, **Muszbek L.** Terminal phase components of the clotting cascade in patients with end-stage renal disease undergoing hemodiafiltration or hemodialysis treatment. *Int J Mol Sci* 21: 8426, 2020. doi:10.3390/ijms21228426.
67. **Flemming S**, **Burkard N**, **Renschler M**, **Vielmuth F**, **Meir M**, **Schick MA**, **Wunder C**, **Germer CT**, **Spindler V**, **Waschke J**, **Schlegel N.** Soluble VE-cadherin is involved in endothelial barrier breakdown in systemic inflammation and sepsis. *Cardiovasc Res* 107: 32–44, 2015. doi:10.1093/cvr/cvv144.
68. **Ponnuchamy B**, **Khalil RA.** Role of ADAMs in endothelial cell permeability: cadherin shedding and leukocyte rolling. *Circ Res* 102: 1139–1142, 2008. doi:10.1161/CIRCRESAHA.108.177394.
69. **Chen B**, **Gao Y**, **Wei S**, **Low SW**, **Ng G**, **Yu D**, **Tu TM**, **Soong TW**, **Nilius B**, **Liao P.** TRPM4-specific blocking antibody attenuates reperfusion injury in a rat model of stroke. *Pflugers Arch* 471: 1455–1466, 2019. doi:10.1007/s00424-019-02326-8.
70. **Chen X**, **Liu K**, **Lin Z**, **Huang K**, **Pan S.** Knockout of transient receptor potential melastatin 4 channel mitigates cerebral edema and neuronal injury after status epilepticus in mice. *J Neuropathol Exp Neurol* 79: 1354–1364, 2020. doi:10.1093/jnen/nlaa134.
71. **Sellers RS.** Translating mouse models. *Toxicol Pathol* 45: 134–145, 2017. doi:10.1177/0192623316675767.
72. **Ariëns RA**, **Lai TS**, **Weisel JW**, **Greenberg CS**, **Grant PJ.** Role of factor XIII in fibrin clot formation and effects of genetic polymorphisms. *Blood* 100: 743–754, 2002. doi:10.1182/blood.v100.3.743.

Downloaded from journals.physiology.org/journal/ajpheart at Bibliotheque Cantonale Et Universitaire (155.105.125.086) on October 18, 2023.